CrossMark
click for updates

View Article Online
View Journal

RSC Advances

This article can be cited before page numbers have been issued, to do this please use: R. N. Chauhan, N. Tiwari, R. S. Anand and J. Kumar, *RSC Adv.*, 2016, DOI: 10.1039/C6RA14124B.

This is an *Accepted Manuscript*, which has been through the Royal Society of Chemistry peer review process and has been accepted for publication.

Accepted Manuscripts are published online shortly after acceptance, before technical editing, formatting and proof reading. Using this free service, authors can make their results available to the community, in citable form, before we publish the edited article. This *Accepted Manuscript* will be replaced by the edited, formatted and paginated article as soon as this is available.

You can find more information about *Accepted Manuscripts* in the Information for Authors.

Please note that technical editing may introduce minor changes to the text and/or graphics, which may alter content. The journal's standard Terms & Conditions and the Ethical guidelines still apply. In no event shall the Royal Society of Chemistry be held responsible for any errors or omissions in this *Accepted Manuscript* or any consequences arising from the use of any information it contains.

ROYAL SOCIETY OF CHEMISTRY

www.rsc.org/advances

 Journal Name RSC Advances
Dynamic Article Links ►
View Article Online
DOI: 10.1039/C6RA14124B

Cite this: DOI: 10.1039/c0xx00000x

www.rsc.org/xxxxxx

ARTICLE TYPE

Development of Al-doped ZnO thin film as transparent cathode and anode for application in transparent organic light- emitting diodes

Ram Narayan Chauhan,*[a] Nidhi Tiwari[d], R. S. Anand[c] and Jitendra Kumar[b]

Received (in XXX, XXX) Xth XXXXXXXXX 20XX, Accepted Xth XXXXXXXXX 20XX
DOI: 10.1039/b000000x

Published on 26 August 2016. Downloaded by Northern Illinois University on 27/08/2016 10:18:48.

Aluminum doped zinc oxide thin films have been prepared by sputtering under argon gas pressure of 0.15 Pa at different radio frequency (R. F.) power density to optimize conditions for application in both bottom emitting and transparent OLEDs. The films exhibit wurtzite-type hexagonal structure with 0002 preferred orientation and optical transmittance of better than 80% in the visible region but varying energy bandgap. The sputtering at high R. F. power density of 2.47 W cm^{-2} yields Al-ZnO films of minimum resistivity (~ 1×10^{-3} Ω cm) and high work function (~ 4.44 eV) and have appropriate for anode in bottom emitting OLEDs. On the other hand, AZO films obtained at low R. F. power density of 0.31 W cm^{-2} correspond to low work function (3.90 eV) with slightly higher electrical resistivity (5.60×10^{-3} Ω cm) and so useful for cathode in transparent OLEDs. The comparable performance observed of OLEDs fabricated with AZO and ITO anode demonstrates suitability of AZO as an alternative electrode. The increase in R. F. power density during sputtering leads to perceptible damage of the organic layer. The introduction of a buffer layer of Alq3/LiF/Al just above the organic layer is shown to suppress the damages significantly and improve the performance of transparent OLEDs.

1. Introduction

Organic light-emitting diodes (OLEDs) have found applications in flat panel displays and solid state lighting applications. They can be classified as bottom emitting or transparent OLEDs depending on emission occurring from the anode or both (anode and cathode) ends.[1] Mg-Ag alloy and double (Li:Al) layers are typically used as cathode. LiF or Cs_2CO_2 is also introduced sometimes between the cathode (Al) and electron transport layer (ETL) for better electron injection efficiency.[2] Indium tin oxide is known anode material for efficient hole injection. Its work function is high (4.5 – 4.6 eV) and can be further improved by oxygen plasma treatment.[3, 4]
The transparent OLEDs emitting light from both sides have applications in double-sided (or head-up) displays and smart windows. Gu et al.,[5] fabricated transparent OLEDs using ITO as anode (or bottom electrode) and a thin layer (thickness ~ 5-40 nm) of Mg-Ag alloy coated ITO as cathode (or top electrode). Zhou et al.,[6] produced an inverted transparent OLEDs based on ITO bottom as cathode and a semi-transparent gold film on top of the organic layer as anode for hole injection. Lim et al.,[7] used a semi-transparent conducting and Cs/Al/Ag protected ITO as cathode and Ag/ITO as anode to get a transparent OLED. The semi-transparent film is employed to protect the organic layer from irradiation of high energy species during deposition of ITO by sputtering. Several transparent cathode materials with conducting protecting layer developed over the years include CuPc/ITO, Li/BCP/ITO, Bphen:Li/ITO, Ag/ITO and Ca/ITO.[8-11] Obviously, ITO is a crucial material for display industry due to its high optical transmittance and low electrical resistivity. However, it contains indium which is toxic, scarce, chemically unstable in reduced environment, and expensive. It can even diffuse to the organic layer causing degradation of OLEDs.[12] This fact and ever increasing demand of industry need replacement of ITO by some in-expensive transparent conducting oxide (TCO). In particular, Al-doped ZnO (abbreviated as AZO) is often considered as good substitute for ITO due to its abundance, high transparency in the visible range, thermal stability, non-toxic nature, and low cost.[13] As anode for bottom-emitting OLEDs, AZO thin films are usually grown above 150°C by a variety of methods, viz., pulsed laser deposition (PLD),[14] atomic layer deposition (ALD),[15] plasma enhanced metal-organic chemical vapor deposition (PE-MOCVD),[16] and sputtering (DC and RF),[17,18]. For example, Jha et al.,[19] prepared AZO thin films of various thicknesses (305 nm – 800 nm) at high substrate temperature (350°C) and obtained minimum electrical resistivity of 1.21×10^{-3} Ω-cm with optical transparency of ~ 86% for 805 nm thick films. Han et al., [20] prepared the AZO thin films under various ambient gases (Ar, Ar + O_2, and Ar + H_2) at 300°C to investigate the influences of the ambient gases, the flow rate of oxygen and hydrogen on the electrical and optical characteristics of the films to be suitable for anode material in OLEDs. The film prepared in Ar + H_2 ambient exhibited minimum resistivity of ~ 3×10^{-3} Ω-cm and optical transmittance of 85% in the visible region. T. Seng et al., [21] studied the thickness dependent electrical and optical properties

RSC Advances Accepted Manuscript

View Article Online
DOI: 10.1039/C6RA14124B

Published on 26 August 2016. Downloaded by Northern Illinois University on 27/08/2016 10:18:48.

of AZO thin films prepared at unheated (30-60°C) and heated (250°C) substrates. The AZO films with heated substrates exhibited the lowest electrical resistivity of 4.15×10^{-3} Ω-cm and average optical transmittance of ~ 92 % in the visible region for thick film (706.3 nm). You et al.,[22] prepared AZO thin film (thickness ~ 200 nm) by pulsed laser co-ablation method and annealed at 450°C in a mixed gas (5% H_2 + 95% N_2) for 1h to result the film with electrical resistivity of 7.54×10^{-4} Ω-cm. Also, Ga-doped and gallium and aluminium co-doped zinc oxide (GAZnO) films usually prepared at higher substrate temperature (>150°C) are considered as much alternative thin films to ITO.[23-30] However, the deposition of transparent conducting cathode over the organic layer in transparent OLEDs is to be processed at relatively low temperatures (i.e., below 80°C) and low r.f. power density to avoid degradation of the organic layer. So, RF sputtering is preferred because of being simple, having better process control, and providing optimum deposition rate to yield smoother film over a large area at a low substrate temperature. Off course, the AZO material is not new and can replace ITO. Also, sputtering is the traditional method to produce its films for TCO applications. While AZO films have largely been deposited above 150°C to obtain desired electrical and optical properties, limited reports exist,[31] with use of low substrate temperatures for the production of AZO film to replace ITO as anode in solar cells and OLEDs. This is challenging task and vital for application of AZO films as anode in flexible opto-electronic devices and as cathode in transparent OLEDs. Hence, an attempt is made here to deposit AZO thin films at ~ 75°C by sputtering with different RF power density to ascertain their suitability as anode and cathode materials for OLED applications. Both bottom and transparent OLEDs based on AZO and commercial ITO electrodes have been fabricated and compared in terms of their characteristics.

2. Experimental details

AZO thin films were deposited on RCA cleaned, air dried, and ozone treated (for 20 min.) glass substrates by RF sputtering using a ZnO:Al_2O_3 (98:2 wt %) target of 99.99% purity procured from Kurtz J Lesker, USA. The substrates were mounted in a holder and held 7 cm away from the target. The chamber was initially evacuated to a base pressure of ~ 2×10^{-6} mbar and then argon gas introduced to maintain a pressure of 0.15 Pa. The deposition was undertaken at RF power density of 0.31, 0.62, 1.23, 1.85, and 2.47 W cm^{-2}; the rate of deposition being 0.1, 0.5, 1.5, 2.3, and 3 Å/s, respectively. The film thickness (~ 400 nm) was controlled by a digital monitor and measured later with a Stylus profiler (Dektak 6M). The substrate was initially held at 25 °C but its temperature rose maximum up to 75°C during deposition of films of thickness 400 nm. A thermocouple is placed inside the working chamber to measure the temperature. The substrate temperature is displayed on a digital temperature indicator.

An X-ray diffractometer (Thermo Electron model ARL X'TRA), an atomic force microscope (Molecular Imaging Pico-SPM), Ocean optic fiber spectrometer model USB 2000, and a four-point probe were employed for phase identification, surface morphology, optical absorption, and sheet resistance measurements, respectively. Carrier concentration of AZO thin films was determined by Hall effect data. The photoluminescence (PL) was

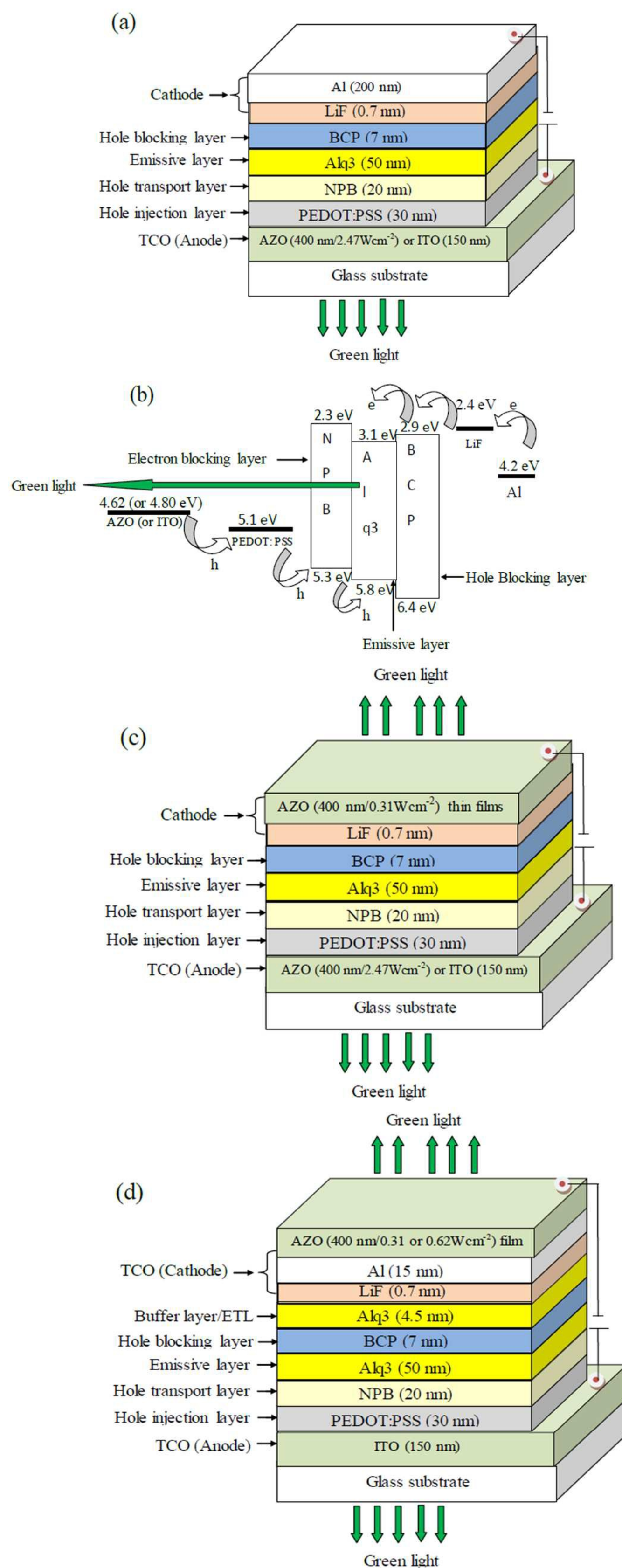

Fig. 1 Schematic diagrams of OLEDs: (a, b) bottom-type with its energy level diagram and (c, d) transparent-type.

RSC Advances Accepted Manuscript

This journal is © The Royal Society of Chemistry [year]

Dynamic Article Links ►
View Article Online
DOI: 10.1039/C6RA14124B

Cite this: DOI: 10.1039/c0xx00000x
www.rsc.org/xxxxxx

ARTICLE TYPE

Published on 26 August 2016. Downloaded by Northern Illinois University on 27/08/2016 10:18:48.

recorded with the Edinburgh Steady state Fluorimeter FS920 to reveal the nature of defects present. The work function was deduced through contact potential difference measurements undertaken with a Kelvin probe-7.

The AZO films deposited with RF power density of 0.62 and 2.47 Wcm^{-2} served as transparent conducting anodes for the fabrication of the OLEDs (bottom emission type) with the process of Zhou et.al,.[32] The patterning was realized by photolithography using shadow mask of size 4 mm × 30 mm. The patterned films were then cleaned gently with tissue paper (dipped in trichloroethylene and acetone) before boiling in isopropyl alcohol for 20 min and treating in ozone for 20 min for removing the organic impurities and increasing the work function. A hole injection layer (thickness ~50 nm) of poly (3, 4-ethylenedioxythiophene) poly (styrenesulphonate) (PEDOT:PSS) was subsequenttly spin coated at 2000 rpm over the AZO films. A 20 nm thin hole transport layer (HTL) of N,N-di(naphth-2-yl)-N,N'-di phenylbenzidine (NPB), a 50 nm thick green color electron emissive layer (EML) of tris (8-hydroxy-quinolinolato) aluminum (III) (Alq3) and a 7 nm thin hole blocking layer (HBL) of 2, 9-dimethyl- 4, 7-diphenylphenanthroline (BCP) were deposited in conjunction by thermal evaporation in vacuum ~ 10^{-6} mbar. Finally, a bilayer of LiF and Al (thickness ~ 0.7 nm and 200 nm, respectively) was thermally laid under vacuum ~ 2 × 10^{-6} mbar over the BCP layer using a mask (8 mm wide × 30 mm long slits) to act as cathode. The structure of the device fabricated with active emission area of 8 mm × 4 mm is shown schematically in Fig. 1(a). For comparative study, another OLED (area ~ 8 mm ×5 mm) was fabricated with the commercial ITO thin films (5 mm wide × 30 mm long pattern size). For transparent OLEDs, LiF/AZO and Alq3/LiF/Al/AZO structures were laid on top of the BCP layer (Fig. 1(c) and (d)). The deposition of LiF or Alq3/LiF/Al layer(s) was made by thermal evaporation in vacuum ~ 2 × 10^{-6} mbar and AZO by sputtering under argon pressure of 0.15 Pa with RF power density of 0.31 and 0.62 W cm^{-2}. The thickness of LiF, Alq3, Al and AZO films were fixed at 0.7, 4.5, 15, and 400 nm, respectively. The OLEDs were analysed for their current density-voltage-luminance (J-V-L) characteristics with a Keithley Source Measure Unit (SMU) and a Minolta Spectro-radiometer (CS-1000A). Also, capacitance-voltage (C-V) measurements of bottom OLEDs were made using an impedance analyzer (Agilent 4294 A).

3. Results and discussion

3.1. Structure, morphology and composition

The XRD pattern of the AZO thin films deposited at RF power density of 0.31 Wcm^{-2} corresponds to wurtzite-type hexagonal structure with [0002] preferred orientation, i.e., the c-axis perpendicular to the substrate (Fig. 2).[33] Notice that the 0002 diffraction peak becomes stronger progressively, shifts towards a higher Bragg angle (2θ) as the RF power density used for film preparation increases, and reaches (2θ = 34.241°) with highest intensity at 1.85 Wcm^{-2}. But, the films produced at power density of 2.47 Wcm^{-2} depict 0002 diffraction peak at a lower angle (2θ = 34.181°) with relatively poor intensity. These results suggest improvement in crystallinity of films only when RF power density employed for deposition increased from 0.31 to 1.85 Wcm^{-2}. Also, the c- parameter decreases with the improvement of crystallinity in AZO films. At higher RF power density, film damage occurs and the lattice parameter increases slightly.[34,35] The optimum RF power density for sputtering seems to be ~ 1.85 Wcm^{-2} for producing AZO films of wurtzite-type hexagonal structure, [0002] preferred orientation and c-parameter 5.233 Å ± 0.001 Å. The average crystallite size (D) as deduced from the Scherrer formula ($D = 0.9\lambda/\beta \cos\theta$; where λ is X-ray wavelength = 1.5406 Å, β is the full width at half maximum of diffraction peak at a Bragg angle θ after correction for instrumental broadening using a standard silicon sample) lies in the range 23-29 nm in sputtered AZO films at RF power density of 0.31, 0.62, 1.23, 1.85, and 2.47 Wcm^{-2}. Table 1 lists the Bragg angles, full width at half maximum data, and the c- parameter of various AZO films along with the RF power density used. Clearly, the (0002) peak shifts to a higher Bragg angle (2θ) with increasing the r.f. power density from 0.31 to 1.85 Wcm^{-2}. This indicates that the adjacent (0002) interplanar distance of AZO films decreases with increase in r.f. power density from 0.31 to 1.85 Wcm^{-2}. This may be related to more aluminum (Al) atoms substitution for zinc (Zn) in ZnO crystal lattice, since the ionic radii of Al^{3+} is smaller (0.054 nm) than that of Zn^{2+} (0.074 nm). While, the (0002) peak seems to be shifted towards lower Bragg's angle (2θ ~ 34.18°) at r.f. power density of 2.47 Wcm^{-2}. Due to limitation of our sputtering system, we could not able to deposit the films over 2.47 Wcm^{-2} to observe and analyze the trend. More data and research over 2.47 Wcm^{-2} are needed in future to observe the exact trend and cause of peak shifting at higher r.f. power density.

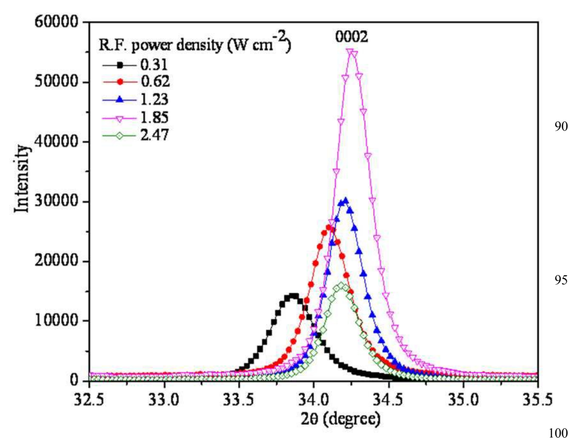

Fig. 2 X- ray diffraction 0002 peak of AZO thin films deposited by sputtering at R.F. power density of 0.31, 0.62, 1.23, 1.85, and 2.47 Wcm^{-2}

RSC Advances Accepted Manuscript

View Article Online
DOI: 10.1039/C6RA14124B

Table 1 Bragg angles (2θ), full width at half maximum (β) and lattice parameter (c) of AZO thin films deposited by sputtering at different R.F. power densities.

R.F. Power density (W cm^{-2})	0.31	0.62	1.23	1.85	2.47
2θ (degree)	33.85	34.10	34.21	34.24	34.18
FWHM (degree)	0.3609	0.3227	0.2983	0.2874	0.2865
Lattice parameter, c ± 0.001, (Å)	5.292	5.254	5.238	5.233	5.242

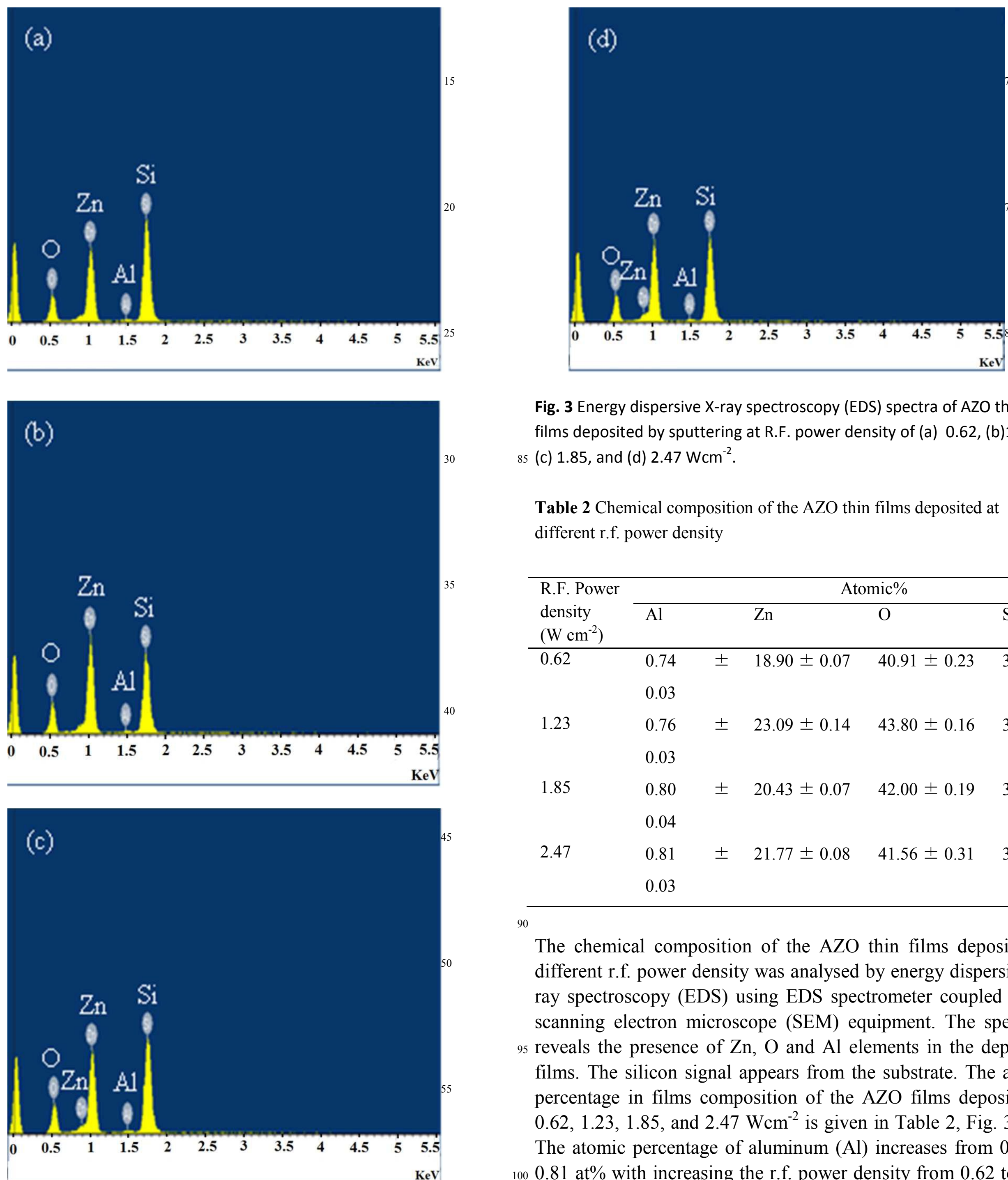

Fig. 3 Energy dispersive X-ray spectroscopy (EDS) spectra of AZO thin films deposited by sputtering at R.F. power density of (a) 0.62, (b)1.23, (c) 1.85, and (d) 2.47 Wcm^{-2}.

Table 2 Chemical composition of the AZO thin films deposited at different r.f. power density

R.F. Power density (W cm^{-2})	Atomic%			
	Al	Zn	O	Si
0.62	0.74 ± 0.03	18.90 ± 0.07	40.91 ± 0.23	39.45 ± 0.22
1.23	0.76 ± 0.03	23.09 ± 0.14	43.80 ± 0.16	32.35 ± 0.20
1.85	0.80 ± 0.04	20.43 ± 0.07	42.00 ± 0.19	36.77 ± 0.15
2.47	0.81 ± 0.03	21.77 ± 0.08	41.56 ± 0.31	35.86 ± 0.20

The chemical composition of the AZO thin films deposited at different r.f. power density was analysed by energy dispersive X-ray spectroscopy (EDS) using EDS spectrometer coupled to the scanning electron microscope (SEM) equipment. The spectrum reveals the presence of Zn, O and Al elements in the deposited films. The silicon signal appears from the substrate. The atomic percentage in films composition of the AZO films deposited at 0.62, 1.23, 1.85, and 2.47 Wcm^{-2} is given in Table 2, Fig. 3(a-d). The atomic percentage of aluminum (Al) increases from 0.74 to 0.81 at% with increasing the r.f. power density from 0.62 to 2.47 Wcm^{-2}, respectively. The EDS mapping (Fig. 4) of the film

This journal is © The Royal Society of Chemistry [year]
Published on 26 August 2016. Downloaded by Northern Illinois University on 27/08/2016 10:18:48.
RSC Advances Accepted Manuscript

Journal Name

RSC Advances

Dynamic Article Links ►
View Article Online
DOI: 10.1039/C6RA14124B

Cite this: DOI: 10.1039/c0xx00000x
www.rsc.org/xxxxxx

ARTICLE TYPE

Published on 26 August 2016. Downloaded by Northern Illinois University on 27/08/2016 10:18:48.

deposited at 0.62 Wcm^{-2} has been performed to look at Al

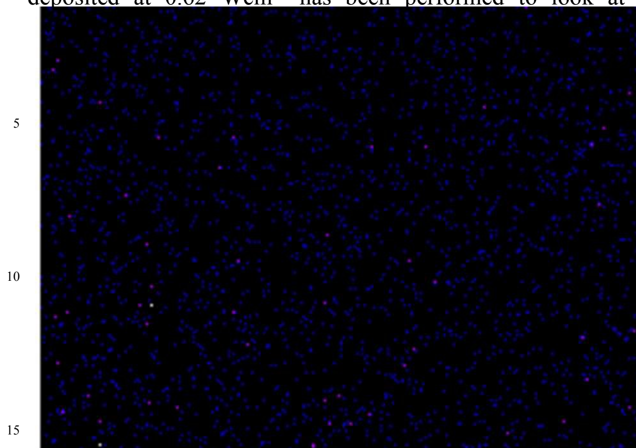

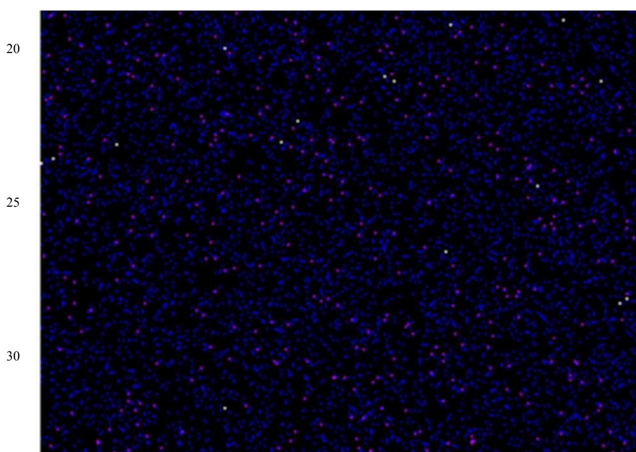

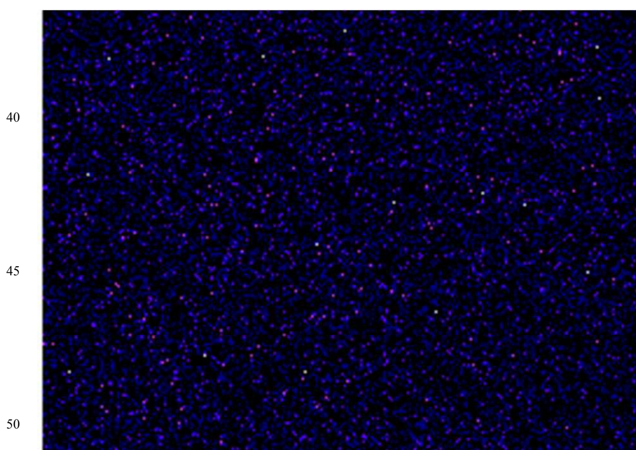

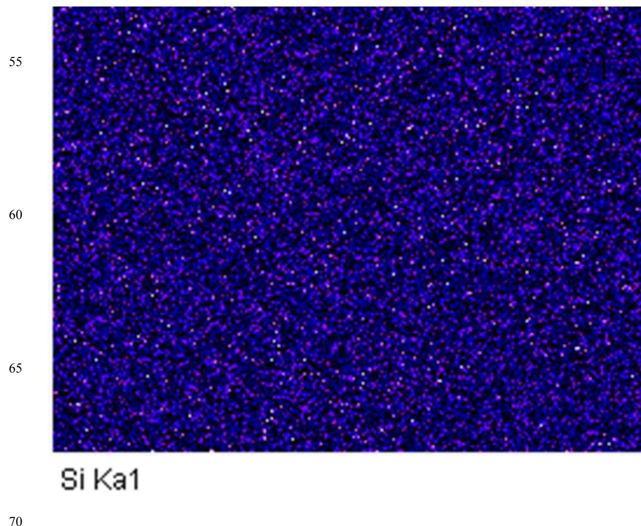

Fig. 4 Energy dispersive X-ray spectroscopy (EDS) mapping of AZO thin films deposited by sputtering at R.F. power density of 0.62 Wcm^{-2} has been performed to look at Al distribution.

Clearly, the microstructure of all samples became uniform, compact interconnected grains, and free of flaws and cracks. By increasing the r.f. power density from 0.62 to 1.85 W/cm^2, the grain size of the AZO thin films increases which can be attributed to the improved mobility of the surface adatoms. Further increase of r.f. power density up to 2.47 W/cm^2 leads to insignificant grain growth. This can be explained in terms of the growing-layer re-sputtering by the highly energetic impinging species.[36] The cross-section SEM images (Fig. 5e-h) of AZO thin films (thickness, t ~ 400 nm) prepared at different r.f. power density exhibited columnar structure with individual columnar grain extending upwards and perpendicular to the substrate. These observations are quite consistent with XRD and AFM analysis.

Three dimensional (3D) AFM images of AZO thin films are shown in Fig. 6. These have been analyzed by a scanning probe image processing (SPIP 6.0.14) software to obtain root-mean square roughness (R_{rms}) data. Accordingly, R_{rms} roughness increases up to a level and lies in the range 1.2-4.5 nm for the case of RF power density of 1.85 Wcm^{-2} but decreases to 2.1 nm at 2.47 Wcm^{-2} due to enhanced re-sputtering perhaps.[36, 37]

3.2. Photoluminescence Studies

Photoluminescence (PL) spectra of AZO thin films obtained with the excitation wavelength of 309 nm are shown in Fig. 7. Note that the AZO film deposited by sputtering at low RF power density of 0.31 Wcm^{-2} exhibits emissions at 395 nm (near band

RSC Advances Accepted Manuscript

View Article Online
DOI: 10.1039/C6RA14124B

Published on 26 August 2016. Downloaded by Northern Illinois University on 27/08/2016 10:18:48.

edge), 405 and 422 nm (violet), 454 nm (blue), and 490 and 541 nm (green). While the near band edge emission ~ 394 nm (3.15 eV) arises due to free exciton recombination and depends on the film crystallinity, the violet emission at 405 nm (3.06 eV)

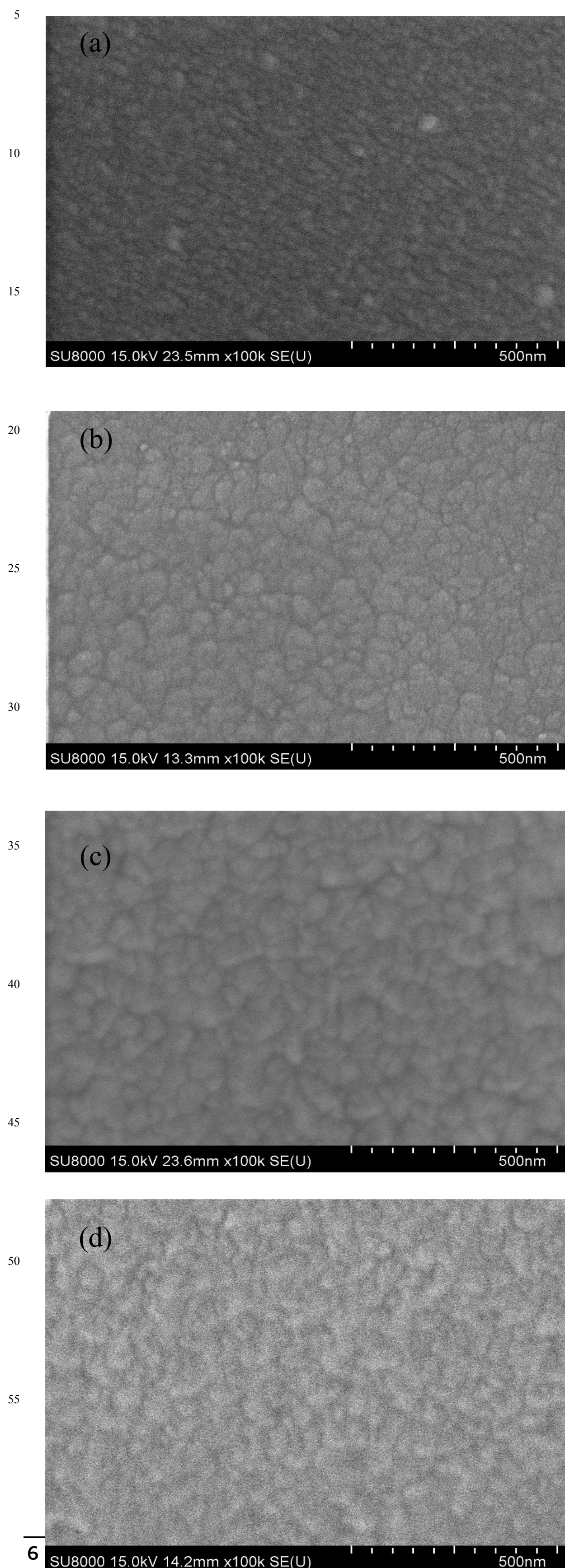

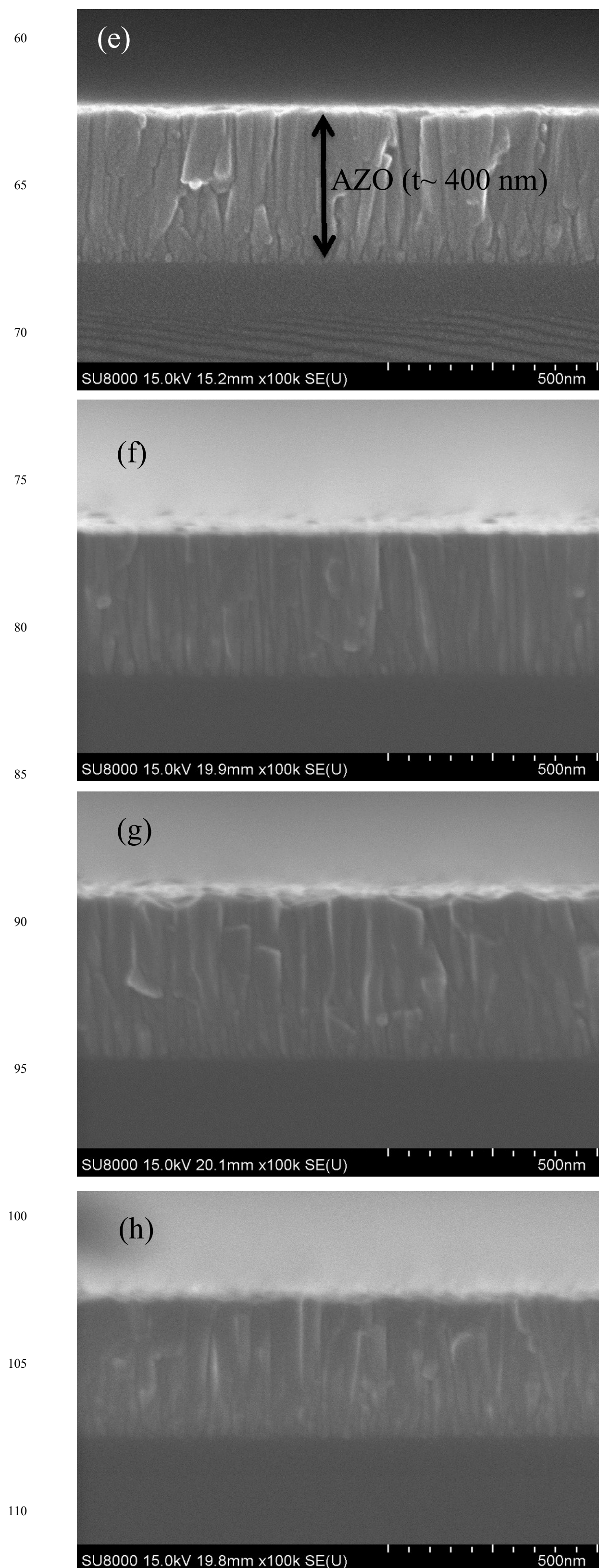

Fig. 5. SEM (micrographs, cross-section) images of AZO thin films (thickness ~ 400 nm) deposited by sputtering at R.F. power density of (a, e) 0.62, (b, f) 1.23, (c, g) 1.85, and (d, h) 2.47 Wcm^{-2}, respectively.

RSC Advances Accepted Manuscript

This journal is © The Royal Society of Chemistry [year]

Dynamic Article Links ►
View Article Online
DOI: 10.1039/C6RA14124B

Cite this: DOI: 10.1039/c0xx00000x

www.rsc.org/xxxxxx

ARTICLE TYPE

Published on 26 August 2016. Downloaded by Northern Illinois University on 27/08/2016 10:18:48.

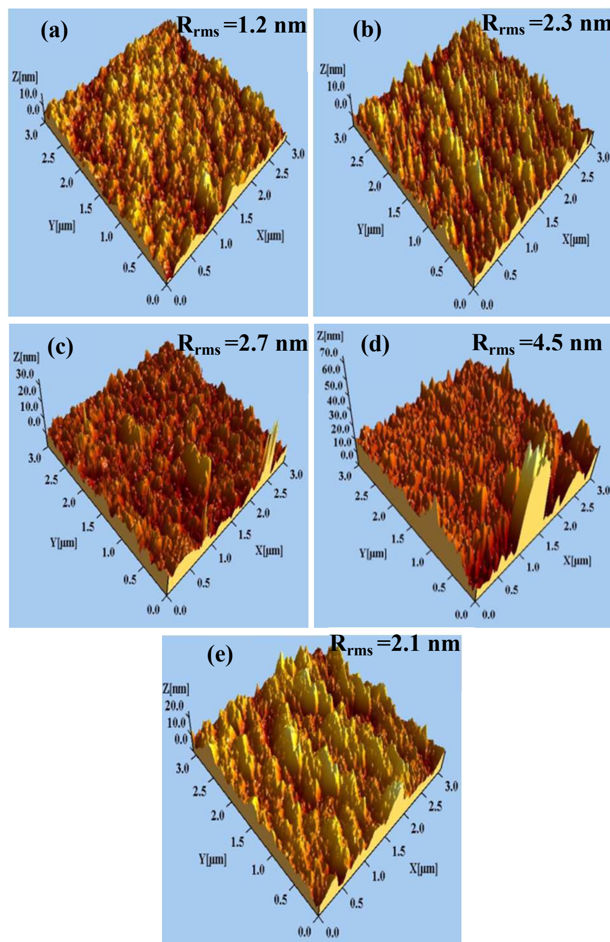

Fig. 6 Three dimensional AFM images of AZO thin films deposited by sputtering at R.F. power density of (a) 0.31, (b) 0.62, (c) 1.23, (d) 1.85, and (e) 2.47 W cm^{-2}.

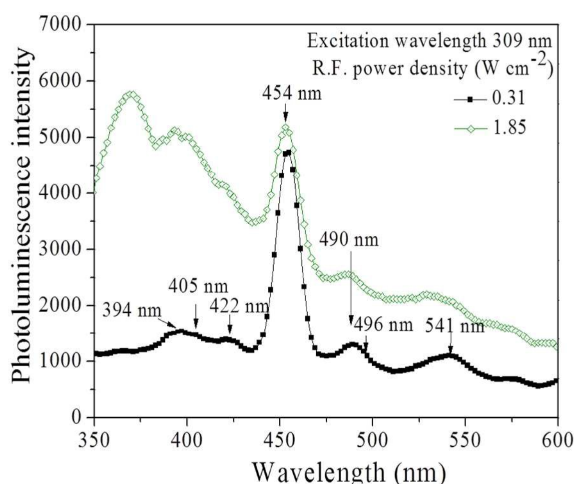

Fig. 7 Photoluminescence (PL) spectra of the R.F. sputtered AZO thin films at r.f. power density of 0.31 and 1.85 Wcm^{-2}.

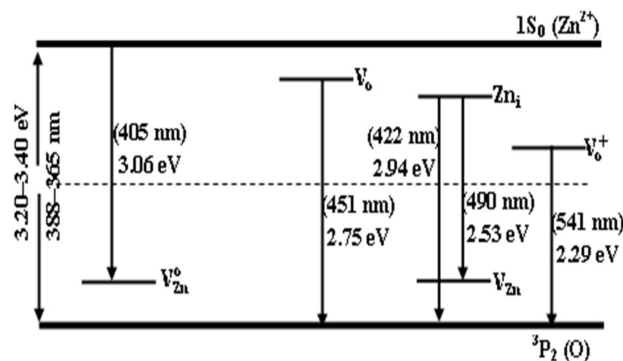

Fig. 8 Schematic diagram of energy levels with possible transitions

is attributed to the transition from conduction band to the energy level of zinc vacancy (V_{Zn}).[38,39] The violet emission at 422 nm is possibly related to transition from zinc interstitial (Zn_i) or interface trap level to the valance band.[40,41] A strong blue emission peak at 454 nm (2.73 eV) results due to transition from shallow donor level of oxygen vacancy (Vo), located at 0.3-0.5 eV below the conduction band, to the valance band.[42] The green emissions at 490 nm (2.53 eV) and 541 nm (2.29 eV) correspond to $Zn_i \rightarrow V_{Zn}$ and recombination of trapped electrons at singly ionized oxygen vacancy (V_o^+) with holes in the valence band, respectively.[43-45] The charge transfer from neutral aluminum (Al_{Zn}^0) to zinc vacancies (V_{Zn}^-) following the reaction $Al_{Zn}^0 + V_{Zn}^- \rightarrow Al_{Zn}^+ + V_{Zn}^{2-}$ gives rise to green PL signal at 496 nm but gets merged with peak arising due to $Zn_i \rightarrow V_{Zn}$ transition around ~490 nm.[46] Fig. 8 shows a schematic diagram of energy levels with possible transitions responsible for various photo-emissions. With increase of RF power density to 1.85 Wcm^{-2}, the resultant AZO films display improved photoluminescence corresponding to blue and green emissions at 2.73 and 2.53/2.29 eV, respectively. This suggests emergence of increasing number of oxygen vacancies and zinc interstitials possibly by irradiation effects. The release of electrons by oxygen vacancies should however increase the overall carrier density. Evidence for this fact is advanced via electrical and Hall measurements of AZO films (Section 3.3). The prominent changes in PL occurring below 454 nm can be related to improved crystallinity of AZO films as mentioned above and revealed by X-ray diffraction as well (Section 3.1) The shift of near band emission towards lower wavelength may be attributed to increase of energy band gap of AZO thin films following rise in carrier concentration through aluminum ion (Al^{3+}) insertion at Zn^{2+} site and creation of additional oxygen vacancies.

3.3. Electrical and optical properties

The sheet resistance ($R_\square$) of AZO thin films deposited by sputtering at different RF power density has been measured by four-point probe. The corresponding electrical resistivity data is deduced from $\rho = R_\square \times t$, where t is the film thickness. Hall

RSC Advances Accepted Manuscript

View Article Online
DOI: 10.1039/C6RA14124B

Cite this: DOI: 10.1039/c0xx00000x

www.rsc.org/xxxxxx

ARTICLE TYPE

Published on 26 August 2016. Downloaded by Northern Illinois University on 27/08/2016 10:18:48.

RSC Advances Accepted Manuscript

Table 3 Electrical and optical parameters of AZO thin films (thickness 400 nm) deposited by sputtering at different R.F. power densities.

R.F. Power density (W cm^{-2})	**0.31**	**0.62**	**1.23**	**1.85**	**2.47**
Sheet resistance ($R_{\square}$) (Ω/square)	140	77	53	27	25
Resistivity (ρ) 10^{-3} (Ω-cm)	5.60	3.08	2.12	1.08	1
Carrier concentration (n) 10^{20} (cm^{-3})	0.60	1.44	3.34	3.98	6.26
Mobility (μ) (cm^2 V^{-1} s^{-1})	18.60	14.09	8.83	14.54	9.98
Optical energy band gap (E_g) (eV)	3.41	3.51	3.57	3.59	3.62
ΔE_{BM} (meV)	170	320	560	630	850
ΔE_{BGN} (meV)	60	110	290	340	530
F_{TC} (10^3 Ω^{-1}cm^{-1})	1.7	3.1	4.5	8.8	9.5
Work function (Φ) (eV)	3.90	3.92	4.40	4.42	4.44

ΔE_{BM} - Burstein-Moss shift, ΔE_{BGN}- Band gap narrowing, F_{TC}-Figure of merit

measurements have been carried out to determine nature of carriers and their concentration (n). Once the electrical resistivity (ρ) and carrier concentration are known, mobility (μ) is obtained using the relation (1/ρ) = neμ, where e is the electronic charge. The experiments revealed n-type conductivity in AZO thin films. The electrical data collected are summarized in Table 3. Notice that the electrical resistivity decreases while the carrier density increases progressively in AZO films with increase in RF power density employed for their deposition. But, the carrier mobility of AZO films decreases with the exception in case of the RF power density of 1.85 Wcm^{-2}, where the value of μ is somewhat higher due to better crystallinity perhaps (Fig. 2). The enhanced electron and ionized impurity scattering of carriers appear to be dominant in reducing the mobility of AZO films.[47] The AZO thin films deposited at r.f. power density of 2.47 W/cm^2 yields lower resistivity of 1.0×10^{-3} Ω-cm. This resistivity value is better than the value (ρ ~ 4.1×10^{-3} Ω-cm) obtained in aluminum and gallium co-doped zinc oxide (GAZnO) thin film prepared by r.f. magnetron sputtering at room temperature using 2wt.% aluminum and 1wt.% gallium as dopants in the ZnO,[48] and comparable to the value (ρ ~ 2.52×10^{-3} Ω-cm) obtained by R. Wu. et. al.,.[49] The high conductivity of the AZO thin films mainly results from non-stoichiometric composition or aluminum doping. Electrons in these films are supplied from donor sites associated with oxygen vacancies or high valence metal ions (Al^{3+}). Therefore the microstructure and doping have a strong influence on the electrical properties of the AZO films. The conductivity of AZO thin film is governed by the carrier concentration and mobility. The high carrier concentration is related to oxygen deficiency and Al^{3+} doping in ZnO. Each oxygen vacancy acts as an ionized donor and contributes one or two free electrons. Also, Al^{3+} substitutes Zn^{2+} and creates a donor level near the conduction band. The grain growth may also release trapped electrons and raise the carrier concentration further. However, the carrier mobility is governed by scattering involving grain boundaries, phonons, electrons and ionized impurities.[50] The grain boundary scattering is expected to be insignificant here as the electron mean free path (L ~ 1 nm) is invariably much smaller than the crystallite size (D ~ 23-29 nm) for the AZO films. Since, the electron concentration of AZO thin films is significant and lies in the range of (n~ 10^{20} - 10^{21} cm^{-3}) with grain size marginally different (D ~ 23-29 nm), electron-electron/impurities scattering mechanism seems to be largely limiting the mobility.[51] The decrease in resistivity despite a decrease in mobility with increase in r.f. power density (Table 3) is because of a disproportionate increase in the carrier concentration following the releases of electrons via oxygen vacancies, Al^{3+} substitution on Zn site, and the grain growth.

The transmittance spectra of AZO thin films deposited by sputtering at different RF power density are shown in Fig. 9. These exhibit average transmittance of ~ 90% in the visible region. Further, the absorption edge shifts towards a lower wavelength (or higher energy) in films produced with increasing RF power density. This possibly happens due to increase in the carrier concentration. The optical energy band gap (E_g) of the film is deduced from the intercept of the linear fit of $(\alpha h\nu)^2$ vs hν or Tauc plot with the energy axis (inset of Fig. 9), where α = (-lnT/t; T is transmittance, t is thickness of film) is absorption coefficient. The resultant values of E_g increase from 3.41 to 3.62 eV with increase in carrier concentration from 6×10^{19} to 6.26×10^{20} cm^{-3} (Table 3). A discussion on the variation in band gap with carrier density,[52-54] and improvement in the figure of merit (F_{TC}),[55] of AZO films with increase in RF power density (Table 3) observed is given in the supporting information (S1).

Dynamic Article Links ►
View Article Online
DOI: 10.1039/C6RA14124B

Cite this: DOI: 10.1039/c0xx00000x

www.rsc.org/xxxxxx

ARTICLE TYPE

Published on 26 August 2016. Downloaded by Northern Illinois University on 27/08/2016 10:18:48.

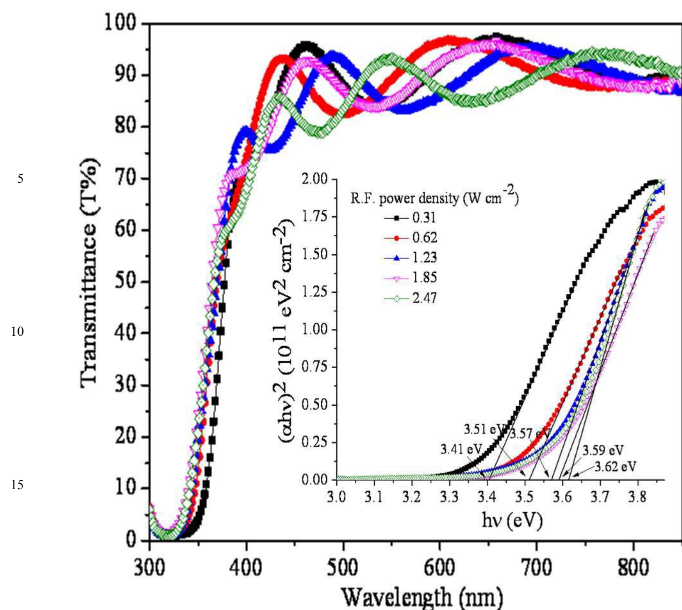

Fig. 9 Optical transmittance spectra of AZO thin films sputtered at various R.F. power densities; inset shows the corresponding $(\alpha h\nu)^2$ versus hν plots.

Kelvin probe measures the average contact potential difference (V_{cpd}) between the tip and the sample following the relation [56]

$$-eV_{cpd} = [\varphi\ \text{tip} - \varphi\ \text{sample}]$$

where φ tip and φ sample represent the work functions of the Kelvin tip and the sample, respectively and e is the electronic charge. An apparent (V_{cpd}) results due to charging of tip and the sample with the existing ac voltage between them. This is nullified by an external bias (V_{dc}) applied in the opposite direction. Under the condition, $V_{cpd} = V_{dc}$, the charges are eliminated altogether and the above expression yields φ sample if φ tip is known. Thus, application of both the ac voltage and external bias (V_{dc}) between the tip and the sample, work function can be deduced with the Kelvin probe when V_{dc} becomes equal to V_{cpd}. Thus, the work function of AZO films deposited by RF sputtering at power density of 0.31, 0.62 1.23, 1.85, and 2.47 Wcm^{-2} are found as 3.90, 3.92, 4.40, 4.42, and 4.44 ± 0.02 eV, respectively (Table 3). The values improve further by 0.2 – 0.3 eV after subjecting films to ozone treatment for 20 min. The above results suggest AZO films sputtered at RF power density of 2.47 Wcm^{-2} can serve as anode (due to their high work function) whereas those produced at low RF power density of 0.31 Wcm^{-2} are suitable for cathode application (work function being smaller) in OLEDs.

3.4. Bottom emitting organic light emitting diodes (BE-OLEDs)

Fig. 10 depicts the capacitance-voltage (C-V) characteristics of

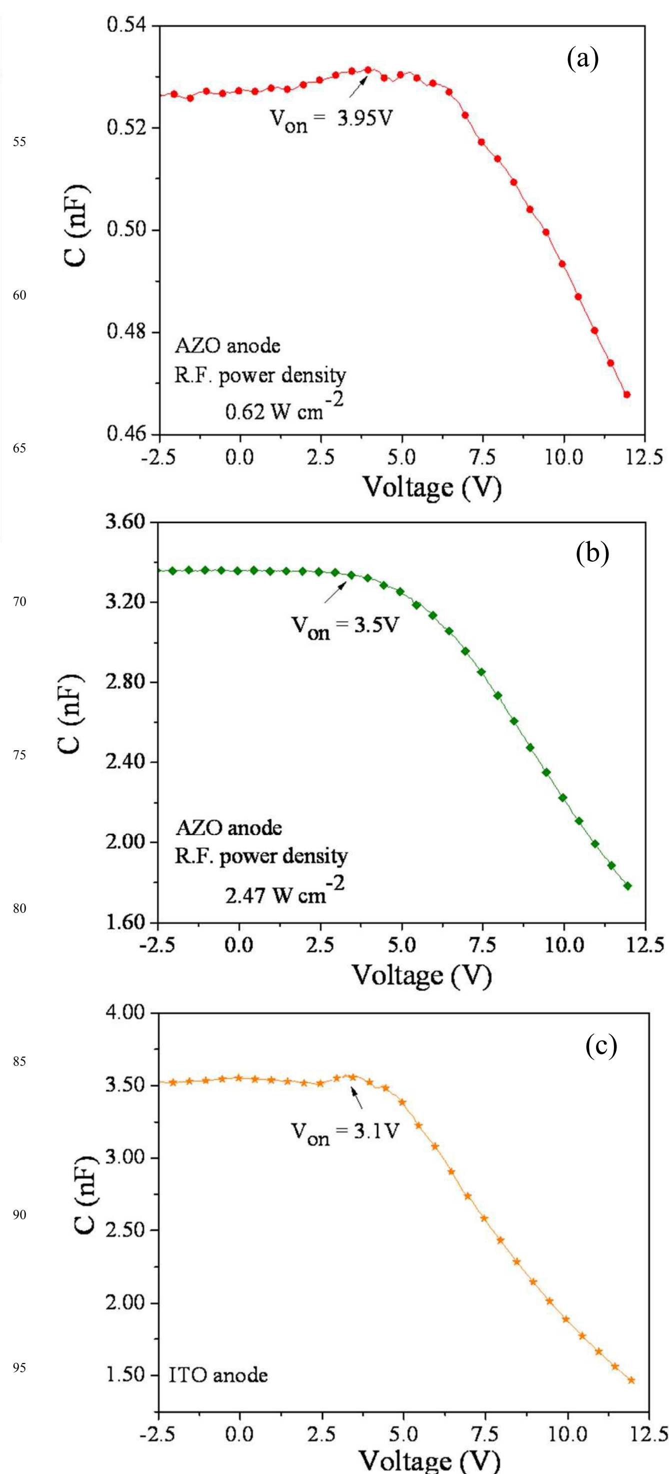

Fig. 10 Capacitance-voltage (C-V) characteristics of some typical bottom emitting OLEDs fabricated with (a, b) R.F. sputtered AZO at power density of 0.62 and 2.47 Wcm^{-2} and (c) commercial ITO thin films as anode.

RSC Advances Accepted Manuscript

View Article Online
DOI: 10.1039/C6RA14124B

Published on 26 August 2016. Downloaded by Northern Illinois University on 27/08/2016 10:18:48.

typical bottom emitting organic light emitting diodes fabricated with AZO thin films, deposited at low (0.62 Wcm^{-2}) as well as high (2.47 Wcm^{-2}) RF power density, as anode. For sake of comparison, a reference device produced with a commercial ITO thin film has also been included in Fig. 10. Note that the device capacitance remains nearly the same or increase marginally up to a certain voltage (~3.1-3.95V) due to accumulation of charge carriers,[57] but, decreases thereafter because of recombination of carriers occurring in the organic layer progressively with emission of light.[58] Also, the turn–on voltage of the devices decrease with increase of the work function (Φ), the values being 3.95 and 3.50 V for Φ equal to 4.22 and 4.62 eV, respectively. The turn-on voltage of the AZO based device is somewhat higher than 3.1 V found in the commercial ITO based device as the R. F. sputtered AZO thin films exhibit lower work function and higher resistivity. The work function (Φ) of commercial ITO film being 4.80 eV.

The current density-voltage-luminance (J-V-L) characteristics of various (AZO / ITO) / PEDOT : PSS / NPB /Alq3/BCP/LiF/Al devices are shown in Fig. 11. Their performance depends on charge injection, balance, and transport.[59,60] Since the hole mobility is high in organic semiconductor, the injection barrier should be comparable or high as compared to cathode to maintain charge balance and ensure recombination efficiency within the emissive layer.[60,61] The variation in the device characteristics with the nature of anode can be noticed in Fig. 11. In case of sputtered AZO films at low R. F. power density, the J-V curves shift towards a higher voltage. The luminance improves with applied voltage in all cases except ITO where increase occurs up to a certain voltage (e.g., ~ 442 Cd/m^2 at ~ 11V) but decreases thereafter. It may happen by charge imbalance resulting with severe injection due to low barrier at anode vis-a-vis cathode.[61,62] As a result, space charge is accumulated near the anode-organic layer interface at higher bias and causes degradation. The performance of OLEDs is measured in terms of luminous flux power efficiency given by $\eta = \pi L/V J = \pi\gamma/V$, where L is the luminance, V is the applied voltage, J is the current density and γ (= L/J) is the luminance current efficiency.[63] The values of η as deduced for bottom OLEDs, fabricated with AZO films (sputtered with r.f. power density of 2.47 Wcm^{-2}) and commercial ITO layers are 0.22 and 0.16 lm/W, respectively at 10V.

J-V characteristics (inset of Fig. 11(a)) of devices follow the power law, $J \alpha V^m$ with m assuming different values depending upon the bias ranges and the power density employed during RF sputtering of AZO films. For example, at low voltages the values of m lie in the range (5-6) when power density varies from 0.62 to 2.47 Wcm^{-2}. However, at higher voltages, it is just 2 for all the cases (inset of Fig. 11(a)). In contrast, the devices with ITO films display correspond to m equal to 4 and 2 at low and high voltage regimes (inset of Fig. 11(a)). These characteristics are consistent with the space charge limited current observed in a trap-filled system.[64-66]

3.5. Transparent organic light emitting diodes

A cathode with low work function and good electron injection characteristics is vital for realizing a transparent organic light emitting diode.[67] Though ITO is used as cathode presently but has high work function which makes that a poor electron injector.[5,8,9] Hence, AZO films deposited by RF sputtering at r.f.

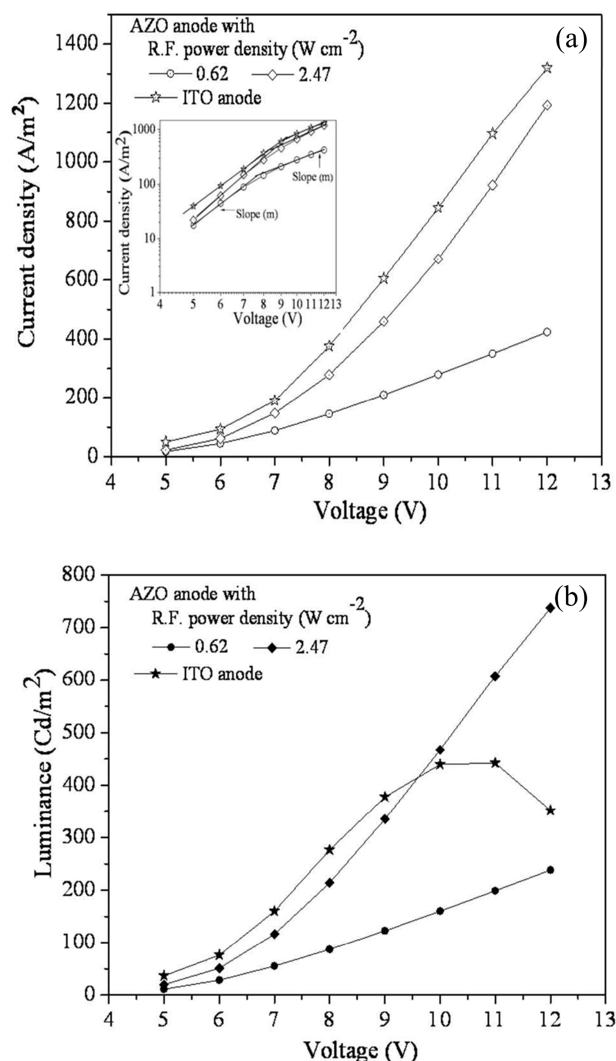

Fig. 11 (a) Current density (J) versus voltage (V) with inset depicting the corresponding plot on log-log scale and (b) luminance versus voltage (L-V) of bottom emitting OLEDs fabricated with R.F. sputtered AZO and commercial ITO thin films as anode.

power density of 0.31 Wcm^{-2} can possibly replace ITO as cathode due to their good electro-optical properties coupled with low work function. On the other hand, AZO films formed at higher power density of 2.47 Wcm^{-2} display high work function (like ITO) and so can serve as alternative anode for OLEDs (Section 3.4). For comparative studies, ITO and AZO anode based transparent OLEDs have been fabricated with AZO thin films, prepared by sputtering at low RF power density of 0.31 Wcm^{-2}, as cathode in both (Section 2). The OLED structure can be expressed as ITO (or AZO/PEDOT:PSS/NPB/Alq3/BCP/LiF/ AZO. The threshold voltage (V_{th}) for initiation of recombination process was somewhat higher (~ 10V) in case of device having AZO anode. With ITO as anode, the device V_{th} was ~ 9V. Such a situation arises due to the difference in work function of ITO and AZO films; values being 4.80 and 4.62 eV, respectively. The current density versus voltage and luminance versus voltage plots of transparent OLEDs fabricated with ITO and AZO thin films as

This journal is © The Royal Society of Chemistry [year]
RSC Advances Accepted Manuscript

Dynamic Article Links ►
View Article Online
DOI: 10.1039/C6RA14124B

Cite this: DOI: 10.1039/c0xx00000x

www.rsc.org/xxxxxx

ARTICLE TYPE

Published on 26 August 2016. Downloaded by Northern Illinois University on 27/08/2016 10:18:48.

anode are shown in Fig. 12(a) and (b), respectively. Their notable features are

a) current density is invariably lower in AZO based OLEDs and increases with increase in forward bias.

b) ITO anode based OLEDs depict different trends in total luminance with the applied voltage, e.g., increase up to a certain voltage and then decrease in the former and increase for the entire range of forward bias (10-15 V) in the later case.

c) total luminance is higher in ITO-based OLED in comparison to AZO-based devices.

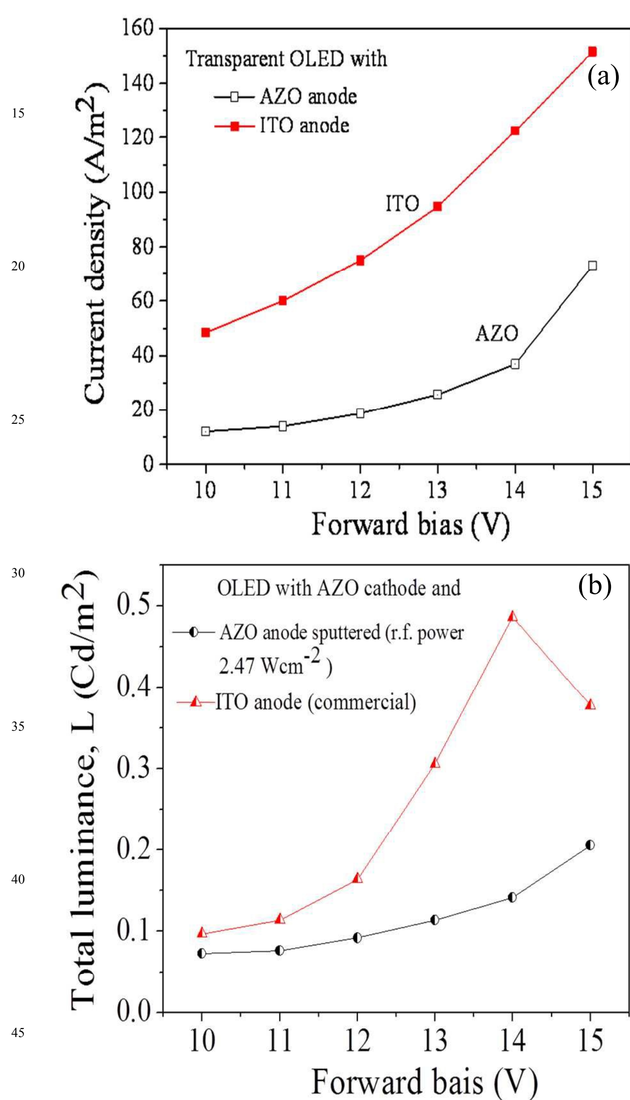

Fig. 12 (a) Current density versus voltage and (b) total luminance versus voltage plots of transparent OLEDs fabricated with ITO and AZO thin films (RF sputtered at power density of 2.47 Wcm^{-2}) as anode; The cathode being AZO thin film sputtered at RF power density of 0.31Wcm^{-2}.

The lower current density of the AZO based transparent OLED can be attributed to (i) lower work function and (ii) high electrical resistivity of AZO films in comparison to ITO. The decrease in luminescence at the anode side in OLED with ITO above 14 V suggests degradation of the devices possibly due to accumulation of holes near the anode and causing increase in the electrical resistivity of the organic layer at a high current density. In contrast, AZO based OLED remains stable. The reason seems to be relatively low work function of AZO films and low current density displayed at high voltages. The reduction in charge carrier injection at the AZO/organic layer interface and, in turn, decrease in the forward current may occur at higher bias following degradation caused by radiation plasma during deposition of AZO films via R.F. sputtering. Also, the sputtered species may penetrate into the organic layer and give rise to high leakage current. Note that the threshold voltage is much higher here than (4 V) found in bottom OLEDs (Section 3.4). It may be due to severe damage of the organic layer at the cathode side during the R. F. sputtering process even though the work function of AZO film is suitable (3.90 ± 0.02 eV) for efficient electron injection.

In both ITO and AZO based devices, the light extraction is less through the top electrode (cathode side) compared to bottom electrode (ITO/AZO anode side) (Fig. 13). As mentioned earlier, it results due to degradation of the AZO - organic layer interface. To protect the organic layer, a buffer multilayer of Alq3 (4.5 nm)/ LiF (0.7 nm)/Al (15 nm) was laid over BCP by thermal evaporation (vacuum level ~ 2 × 10^{-6} mbar). LiF not only improves the electron injection but also prevents diffusion of aluminum species into the BCP layer. An additional Alq3 layer is used for further protection of the BCP. To demonstrate the degradation effect clearly, AZO film was deposited as cathode by R. F. sputtering at power density of 0.31 and 0.62 Wcm^{-2} in ITO anode based

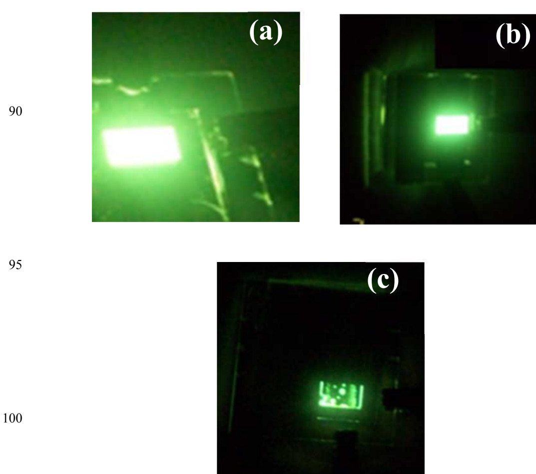

Fig. 13 Photographs of the transparent OLEDs with light emanating towards (a) ITO anode, (b) AZO anode and (c) AZO cathode.

RSC Advances Accepted Manuscript

View Article Online
DOI: 10.1039/C6RA14124B

Published on 26 August 2016. Downloaded by Northern Illinois University on 27/08/2016 10:18:48.

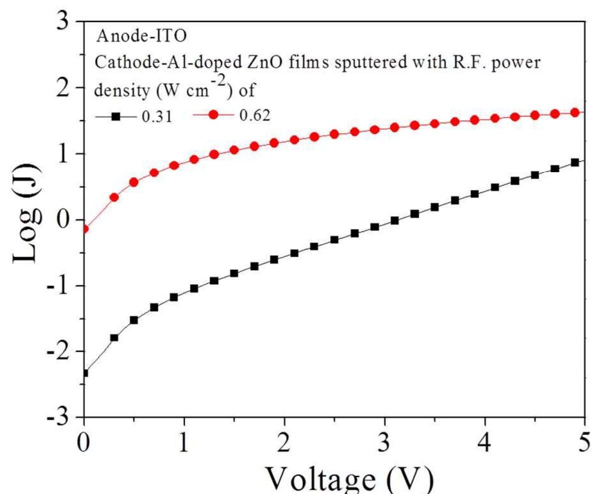

Fig. 14 Current density versus voltage (J-V) characteristics of transparent OLEDs fabricated with sputtered AZO films at R.F. power density of 0.31 and 0.62 W cm^{-2} as cathode and ITO as anode.

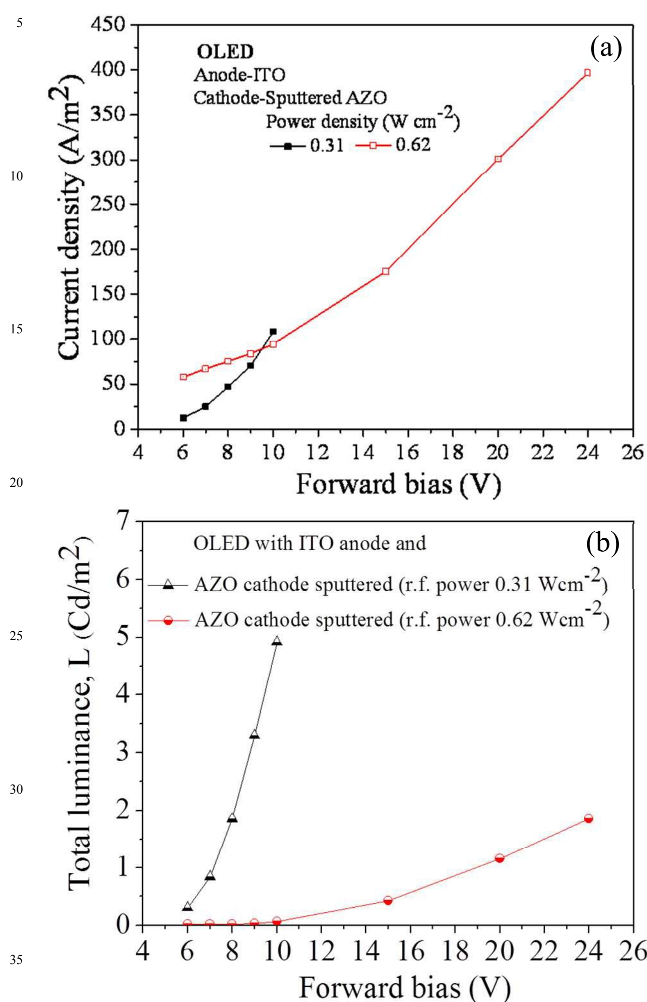

Fig. 15 (a) Current density versus voltage plots of transparent OLEDs fabricated with ITO as anode and R.F. sputtered AZO thin films at power density of 0.31 and 0.62 Wcm^{-2}) as cathode and (b) their total luminance emanating as a function of forward bias.

devices. The J-V characteristics of the resulting ITO/ PEDOT:PSS/ NPB/ Alq3/BCP/Alq3/LiF/Al/AZO devices are shown in Fig. 14. Note that the device with AZO cathode produced at higher power density shows higher leakage current density (J = 0.72 A/m^2) presumably due to massive damage of the organic layer caused even with the buffer layer in place. The leakage current reduces by two order of magnitude (~ 4.7 × 10^{-3} A/m^2) when R. F. power density is made half. Further, the threshold voltage (V_{th}) decreases from 10V to 5V while the work function of AZO film remains essentially the same at ~ 3.92 ± 0.02 eV. The J-V-L characteristics of OLEDs have been presented in Fig. 15. The total luminance is higher in devices having AZO films deposited by RF sputtering at lower power density. The comparison of devices further reveal that insertion of a buffer layer lowers the threshold voltage from 9 V to 5 V in case of AZO film deposited by R. F. sputtering at the lowest power density of 0.31 Wcm^{-2}. The above results clearly indicate effectiveness of Alq3/LiF/Al buffer layer in protecting the organic layer during the deposition process of AZO films by R. F. sputtering.

4. Conclusions

Transparent conducting AZO thin films deposited by R. F. sputtering at power density of 2.47 W cm^{-2} and low substrate temperatures (75°C) can be alternative to ITO as anode for bottom emitting OLEDs. The devices fabricated with AZO anode exhibit good charge balance, improved stability even at high current density, but a high turn-on voltage. The AZO films sputtered at a low power density (0.31 Wcm^{-2}) correspond to low work function, act as efficient electron injector and so suitable for cathode of transparent OLEDs. The increase in R. F. power density during sputtering of AZO films leads to perceptible damage of the organic layer which, in turn, is responsible for raising the threshold and turn-on voltage of a transparent OLED. The introduction of a buffer layer of Alq3/LiF/Al just above the organic layer reduces the damages considerably, lowers the turn-on voltage, and improves the performance of transparent OLEDs.

Notes and references

[*a] *Department of Physics. National Institute of Technology Patna, Patna-800005, India, Tel: +917635052020; E-mail: ramncproject@gmail.com*
[b] *Materials Science Programme. Indian Institute of Technology Kanpur, Kanpur-208016, India, Fax: +91-0512-2597664; Tel: +91-512-2597107; E-mail: jkiitk@gmail.com,*
[c] *Department of Electrical Engineering. Indian Institute of Technology Kanpur, Kanpur-208016, India, Fax: +91-0512-2590063; Tel: +91-512-2597102; E-mail: rsanand@iitk.ac.in*
[d] *,Department of Photonics and Display Institute, National Chiao Tung University, Taiwan, E-mail: nidhi1611@gmail.com*

1 J. Lee, S. Hofmann, M. Furno, M. Thomschke, Y. H. Kim, B. Lüssem and K. Leo, *Org. Electron.*, 2011, **12**, 1383.
2 J. Huang, G. Li, E. Wu, Q. Xu and Y. Yang, *Adv. Mater*., 2006, **18**, 114.
3 W. Brutting, S. Berleb and A. G. Muckl, *Org. Electron., 2001, **2**, 1.*
4 C.C. Wu, C. I. Wu, J. C. Sturm, and A. Kahn, *Appl. Phys. Lett.,* 1997, **70**, 1348.
5 G.Gu, V. Bulovic, P. E. Burrows, S. R. Forrest and M. E. Thompson, *Appl. Phys. Lett.,* 1996, **68,** 2606.
6 X.Zhou, M. Pfeiffer, J. S. Huang, J. B. Nimoth, D. S. Qin, A. Werner, J. Drechsel, B. Maennig and K. Leo, *Appl. Phys. Lett.,* 2002, **81**, 922.

RSC Advances Accepted Manuscript

This journal is © The Royal Society of Chemistry [year]

Dynamic Article Links ►
View Article Online
DOI: 10.1039/C6RA14124B

Cite this: DOI: 10.1039/c0xx00000x

www.rsc.org/xxxxxx

ARTICLE TYPE

Published on 26 August 2016. Downloaded by Northern Illinois University on 27/08/2016 10:18:48.

7 J. T. Lim, C. H. Jeong, M. S. Kim, J. H. Lee, J. W. Bae and G. Y.Yeom, *J. Korean Phys. Soc.*, 2007, **51**, 1147
8 G. Parthasarathy, P. E. Burrows, V. Khalfin, V. G. Kozlov and S. R. Forrest, *Appl. Phys. Lett.*, 1998, **72**, 2138.
9 G. Parthasarathy, C. Adachi, P. E. Burrows and S. R. Forrest, *Appl. Phys. Lett.*, 2000, **76**, 2128.
10 H. Kanno,Y. Sun and S. R. Forrest, *Appl. Phys. Lett.,* 2005, **86**, 263502.
11 M.-H. Lu, M. S. Weaver, T. X. Zhou, M. Rothman, R. C. Kwong, M. Hack and J. J. Brown, *Appl. Phys. Lett.,* 2002, **81**, 3921.
12 J.-H. Lee, J. J. Huang, C.-C. Liao, P.-J. Hu and Y. Chang, *Chem. Phys. Lett.,* 2005, **402**, 335.
13 H. Chen, Y.-H. Jeong and C.-B. Park, *Trans. Electr. Electron. Mater.,* 2009, **10**, 58.
14 H. Kim, A. Piqu, J. S. Horwitz, H. Murata, Z.H. Kafafi, C.M. Gilmore and D.B. Chrisey, *Thin Solid Films,* 2000, **377**, 798.
15 S. C. Gong, Y.-J. Choi, H. Kim, C.-S. Park, H.-H. Park, J. G. Jang, H. J. Chang and G. Y. Yeom, *J. Vac. Sci. Technol. A,* 2013, **31**, 01A101.
16 I. Volintiru, M. Creatore, B. J. Kniknie, C. I. M. A. Spee and M. C. M. van de Sanden, *J. Appl. Phys.,* 2007, **102**, 043709.
17 X. Jiang, F. L. Wong, M. K. Fung and S. T. Lee, *Appl. Phys. Lett.,* 2003, **83**, 1875.
18 D. Xu, Z. Deng, Y. Xu, J. Xiao, C. Liang, Z. Pei and C. Sun, *Phys. Lett. A,* 2005, **346**, 148
19 J. K. Jha, R. Santos-Ortiz, J. Du, N. D. Shepherd, *J Mater Sci: Mater Electron* 2014, **25**, 1492
20 S. -H. Han, D. –B. Jo, K. –M. Le, *Electron. Mater. Lett.*, 2013, **9(S),** 43
21 Z. –L. Tseng, P. –C. Kao, Y. –C. Chen, Y. –D. Juang, Y. –M. Kuo, S. –Y. Chu, *J. Electrochem. Soc*,2011, **158**, J310
22 Q. You, H. Cai, K. Gao, Z. Hu, S. Guo, P. Liang, J. Sun, N. Xu, J. Wu, *J. Alloys Compd*, 2015, **626**, 415
23 C.-C. Chen, H.-C. Wu, *Materials,* 2016, **9**, 164
24 R. Ebrahimifard, M. R. Golobostanfard, H. Abdizadeh, *Appl. Surf. Sci.,* 2014, **290**, 252
25 W. Lee, S. Shin, D. R. Jung, J. Kim, C. Nahm, T. Moon, B. Park, *Curr. Appl. Phys,. 2012*, **12**, 628
26 J. H. Shin, D. K. Shin, H. Y. Lee, J. Y. Lee, N. I. Cho, S. J. Lee, *J. Korean Phys. Soc.*, 2009, **55**, 947
27 J. Liu, W. J. Zhang, D. Y. Song, Q. Ma, L. Zhang, H. Zhang, X. B. Ma, H. Y. Song, *Ceram. Int.*, 2014, **40**, 12905
28 Z. Y. Zhang, C. G. Bao, S. Q. Ma, S. Z. Hou, *Appl. Surf. Sci.*, 2011, **257**, 7893
29 M. Bazzani, A. Neroni, A. Calzolari, A. Catellani, *Appl. Phys. Lett.* 2011, **98**, 121907
30 M. H. Lee, , Y. C. Peng, H. C. Wu, *J. Alloys Compd.,* 2014, **616**, 122
31 Z. –L. Tseng, P. –C. Kao, C. –S. Yang, Y. –D. Juang, S. –Y. Chu, *Appl. Surf. Sci.,* 2012, **261**, 360
32 G.-J. Zhou, W.-Y. Wong, B. Yao, Z. Xie and L. Wang, *J. Mater. Chem.,* 2008, **18**, 1799.
33 N. Fujimura, T. Nishihara, S. Goto, J. Xu and T. Ito, *J. Cryst. Growth,* 1993, **130**, 269.
34 M. K. Puchert, P. Y. Timbrell and R. N. Lamb, *J. Vac. Sci. Technol. A,* 1996, **14**, 2220.
35 Z.B. Fang, Z.J. Yana, Y.S. Tan, X.Q. Liua and Y.Y. Wang, *Appl. Surf. Sci.,* 2005, **241**, 303.
36 L. Monteagudo-Lerma, S. Valdueza-Felip, A. Núñez-Cascajeroa, M. González-Herráez, E. Monroy, F.B. Naranjo, *Thin Solid Films* 2013, **545**, 149
37 H. Chou, P. I. Lin, C. C. Hsu, T. C. Chow, M. T. Hong, Y. C. Chen, J. R. Liu and T. P. Tsai, *J. Vac. Sci. Technol. A,* 2002, **20**, 441.
38 Y.H. Yang, H.G. Zhu and G.W. Yang, *Appl Phys A,* 2011, **103**, 3.
39 B. Lin, Z. Fu and Y. Jia, *Appl. Phys. Lett.,* 2001, **79**, 943.
40 N. Boukos, C. Chandrinou, K. Giannakopoulos, G. Pistolis and A. Travlos, *Appl. Phys. A,* 2007, **88**, 35.
41 X.Q. Wei, B.Y. Man, M. Liu, C.S. Xue, H.Z. Zhuang and C. Yang, *Physica B*, 2007, **388**, 145.
42 Q.P. Wang, D.H. Zhang, H.L. Ma, X.H. Zhang and X.J. Zhang, *Appl. Surf. Sci.,* 2003, **220**, 12.
43 U. Ilyas, R. S. Rawat, T. L. Tan, P. Lee, R. Chen, H. D. Sun, Li Fengji and Sam Zhang, *J. Appl. Phys.,* 2011, **110**, 093522.
44 Y. Hu and H.-J. Chen, *J. Nanopart. Res.,* 2008, **10**, 401.
45 A. Ghosh and R N P Choudhary, *J. Phys. D: Appl. Phys.,* 2009, **42**, 075416.
46 Z. -Z. Li, M. Bao, S.-H. Chang, Z.-Z. Chen, and X.-M. Ma, *Vacuum,* 2012, **86,** 1448
47 D.H. Zhang and H.L. Ma, *Appl. Phys. A,* 1996, **62**, 487.
48 B. Onwona-Agyeman, M. Nakao, T. Kohno, D. Liyanage, K. Murakami, T. Kitaoka, *Chem. Eng. J.,* 2013, **219,** 273
49 R. Wu, W. Zhang, H. Zhang, D. Song, Q. Ma, J. Liu, X. Ma, L. Zhang, L. Zhang, H. Song, *Mater Sci Semicond Process,* 2014 , **19**, 24
50 D. H. Zhang, H. L. Ma, *Appl. Phys. A.,* 1996, **62**, 487
51 K. L. Chopra, S. Major, D. K. Pandya, *Thin Solid Films* 1983, **102**, 1
52 M. Caglar, S. Ilican, Y. Caglar and F. Yakuphanoglu, *Appl. Surf. Sci.,* 2009, **255**, 4491.
53 S.-M. Park, T. Ikegami, K. Ebihara and P.-K. Shin, *Appl. Surf. Sci.,* 2006, **253**, 1522.
54 J. Kumar, A. K. Srivastava, *J. Appl. Phys.,*2014, **115**, 134904.
55 R E. I. Schropp, A. Madan, J. Appl. Phys., 1989, **66**, 2027.
56 W. Melitz, J. Shena, A. C. Kummel, S. Lee, *Surface Science Reports*, 2011, **66**, 1
57 B. G. Streetman and S. K. Banerjee, *Solid state electronic devices*, Pearson Education, Inc. and Dorling Kindersley (India) Pvt. Ltd., 2007.
58 L. Zhang, H. Nakanotani and C. Adachi, *Appl. Phys. Lett.,* 2013, **103**, 093301.
59 C. Qiu, H. Chen and M. Wong, *IEEE Trans. Electron Devices,* 2001, **48**, 2131.
60 A. Benor, S.-y Takizawa, C. P. Bolivar and P. Anzenbacher, *Appl. Phys. Lett.,* 2010, **96**, 243310
61 T. Mori, H. Fujikawa, S. Tokito and Y. Taga, Appl. Phys. Lett., 1998, **73**, 2763.
62 P. Kumar, A. Misra, M N Kamalasanan, S C Jain and V. Kumar, *J. Phys.D: Appl. Phys.,* 2007, **40**, 561.
63 C. Qiu, H. Chen, M. Weng, and H. S. Kwok, *IEEE Trans. Electron Devices,* 2001, **48**, 2131–2137
64 A. A. A. Ghamdia, O. A. A. Hartomya, B. M. Cavasc, F. E. Tantawyd and F. Yakuphanoglue, *Optoelectron. Adv. M.,* 2012, **6**, 292.
65 W. Chandra, L. K. Ang, K. L. Pey and C. M. Ng, *Appl. Phys. Lett.,* 2007, **90**, 153505.
66 P. E. Burrows and S. R. Forrest, Appl. Phys. Lett., 1994, **64**, 2285.
67 M. Pfeiffer, S.R. Forrest, X. Zhou and K. Leo, *Org. Electron.,* 2003, **4**, 21.

RSC Advances Accepted Manuscript